Annals Geol. Surv. Egypt. XL (2024). pp. 148- 163
Manuscript ID: ASGE-2411-1026

# Geology, Remote Sensing and Geophysical Studies of Atshan Area, South Eastern Desert, Egypt.

**BY**

Mahdy Kh. Abd- El Sadek [1 *] Adel A. A. Othman [2], S. A. S. Araffa [3] and Waheed H. Mohamed[2]

1. Egyptian Mineral Resources Authority, |EMRA| Cairo. Egypt.
2. Geology Department Faculty of Science, Al – Azher University, Cairo. Egypt.
3. National Research Institute of Astronomy and Geophysics | NRIAG|, Helwan, Cairo, Egypt.

Mahdykhamis85@gmail.com

**ABSTRACT**

*In this study we focusing on the occurrences of mineralized zones, which are composed of metavolcanic rocks (metarhyolite, metaandesite, and metebasalt), to explore sulfide mineralization and its gold related of them. To achieve this target, we applied various methods such as: remote sensing, magnetic survey, self-potential (SP) and 2D geoelectrical profiles to outline the mineral resources in depths and extensions which there are in the structural control (faults and shearing zones). The processing and interpretation of magnetic measurements were made by using several methods; such as Reduced to the northern pole (RTP), low-pass (regional) and band -pass magnetic maps using the (Geosoft Oasis Montag-2015) program. The results indicated that high magnetic potentialities (up to 41563 nT) are concentrated in the central, southeastern and southwestern parts, these high magnetic anomalies correspond to metavolcanic rocks and the delineating depths may be range from range from 5 to 30 m. The SP shows negative anomalies occupy the high stain zones (mainly silicified and alterations zones). Also, the low-SP zones coincide with other geophysical anomalies and geological signature of metavolcanics rocks cropping out in the study area. Two Geo-electric cross section were acquired along the magnetic and SP anomalies to know more detailed information*

***Key Words:*** Mineral occurrences, Ground magnetic, Self-Potential, 2-D Geoelectrical profile.

## INTRODUCTION

The investigated Atshan area is located in the Hamata region. The area lies between longitudes 35° 05` 00" and 35° 20` 00" E and latitudes 24° 10` 00" and 24° 20` 00" N, (Fig.1). It is located 95km south of Marsa Alam. This area has been intensively investigated by many Authors (e.g. Elnazer, et al., 2022 and Hamdy et al.., 2022)**.** In this study, integrated of geological, remote sensing analysis and ground geophysical surveys were done to investigate the mineral occurrences in metavolcanics.

## GEOLOGIC SETTING

The Hamata region has been extensively studied and investigated by several authors: Shukri and Mansour (1980), Abu El-Rus (1991), EGSMA (1997) and El-Bialy, M.Z. (2010).

The metavolcanics classified into, basic and intermediate types including metabasalts, and metaandesits and acid varieties including metarhyolites and metarhyodacites (El-Ramly and Akaad, 1960). From the field investigations and the light of the results of previous work, we selected area of study. The area is dissected by many fracture sets (dikes and faults) mainly of NE-SW and E-W. They range in length from few centimeters scale to tens of meters. Most of NE-SW faults have been clearly identified as normal faults. Some E-W faults are strike slip with dextral sense of movement. Thrust faults are recognized in the metavolcanics along E-W shear zone at Atshan area. The basement rocks

are mainly Island arc metavolcanics, Arc granitoids (Tonalite and granodiorite), continental margin volcanic (Dokhan volcanics), Hammamat sediments, younger gabbros and Monzo to Alkali feldspar granites all these rocks dissected by quartz veins and dikes (Fig.2). These rock units are described in some detailed, from oldest to youngest.

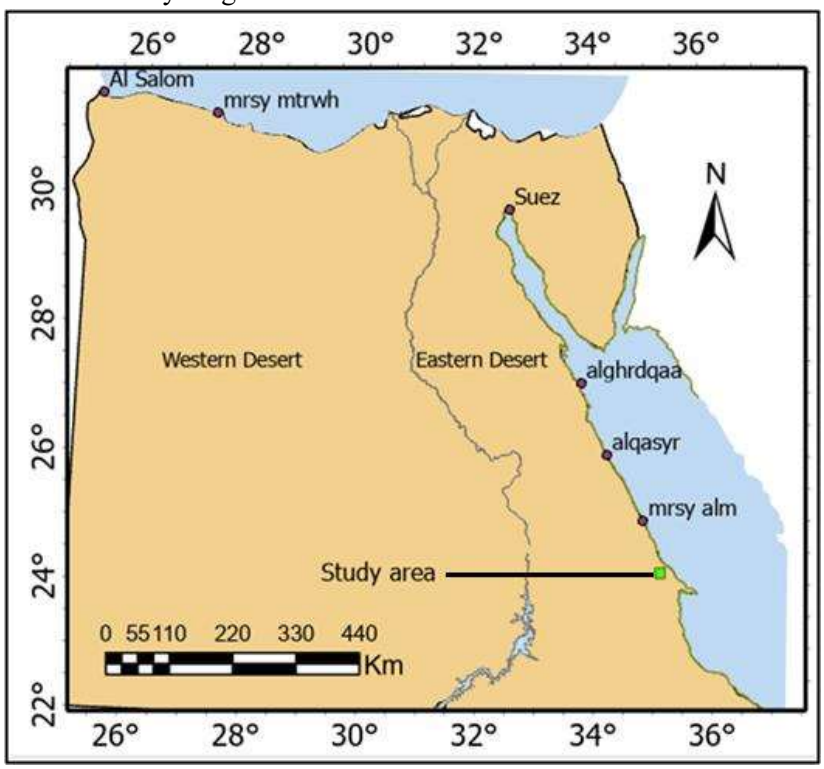


Fig.1 Location map of investigated area.

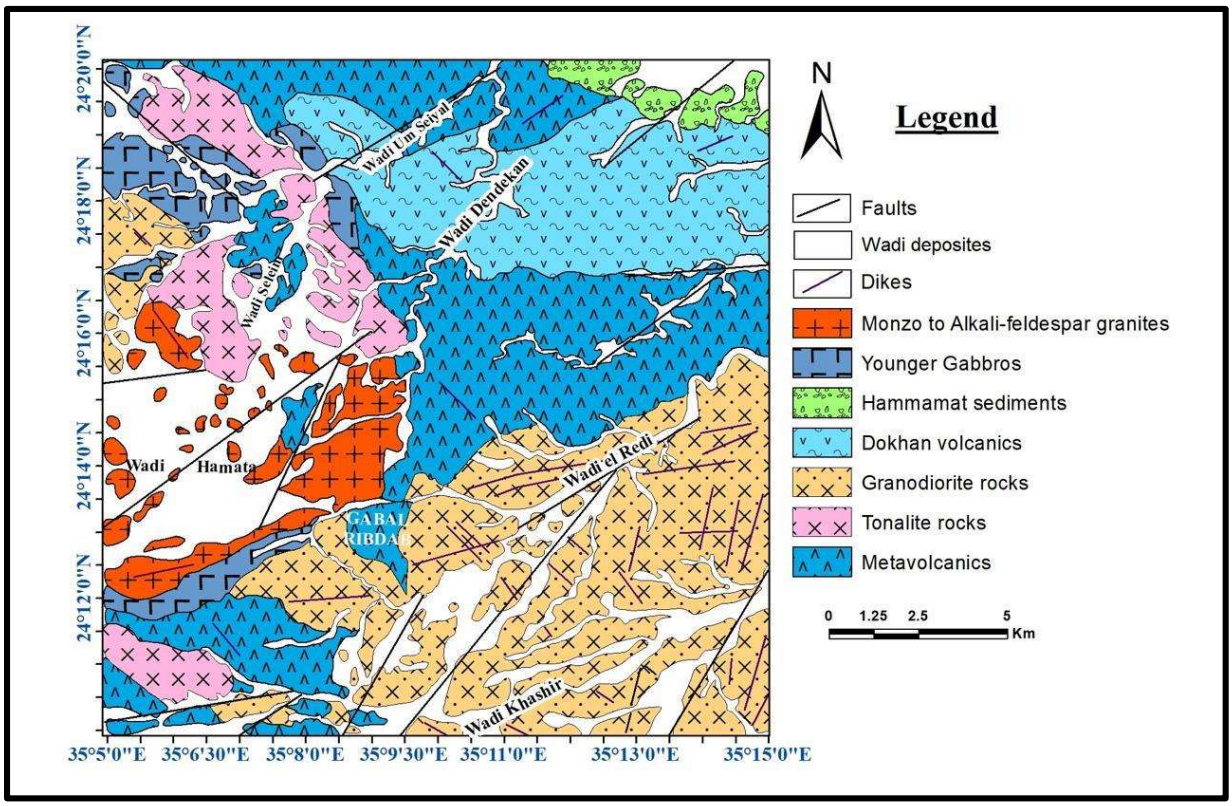


Fig.2 Geological map of the study area (after EGSMA,1994 and 1996)

**Island Arc Metavolcanics**

Island arc rocks occupy the central, northeastern and southwestern portions (see Fig. 2), which are basic to intermediate metavolcanic rocks. They are highly sheared and foliated along the shear zones and cut by many quartz veins and dissected by many joints (Fig. 3).

Fig.3 Shearing in arc metavolcanics in Wadi Qulan el Atshan (Looking SW).

**Arc Granitoids (Tonalites and Granodiorites)**

These rocks are mainly observed in the west, northwestern and southeastern portions of the present study (see Fig. 2) and occurred as oval and elongated masses forming low to moderately relief and referred to as syn-orogenic plutonite (El Shazly, 1964) and (Akaad and Noweir, 1980). They show well developed spheroidal weathering (Fig.4), Tonalites and granodiorites are highly jointed, and dissected by numerous quartz veins.

Fig.4 Granodiorites showing a well-developed spheroidal weathering

**Continental Margin Volcanic (Dokhan Volcanics)**

These rocks form moderate hilly terrain with different shades of purple, red, yellow, grey, green and black. They include acidic and intermediate volcanics.

**Hammamat Sediments**

Hammamat sediments are restricted to the extreme northeastern part and observed as a narrow strip propagating along the NW-SE trend. The Hammamat sediments comprise distinctive well bedded, immature, poorly-sorted molasse sediments.

**Younger Gabbros**

The younger gabbros are generally unmetamorphosed; they are post-tectonic rock units, (El-Ramly, 1972) but El-Gaby et al. (1988) grouped them into syn-to-late-orogenic plutonites.

Abu ElLeil, 1990 the non-metamorphosed relics of troctolite and olivine gabbro occur either within the metagabbro and metagabbro norite, forming linear and arch-shaped bodies, or in close proximity to them, forming usually isometric bodies.

**Monzo To Alkali Feldspar Granites**

The late-tectonic (suture related granites) granites; known as the within plat-younger (Pink) granites, which range in age from 530-620 Ma (Hassan and Hashad, 1990). These rock units formed mainly in the shape of medium to low masses in central and central-western portions and intrudes the island arc metavolcanic rocks (Fig.5). This rock is creamy white in color, coarse to medium-grained and shows well developed spheroidal weathering. Several workers have already taken interest in the ore genesis of the Precambrian polymetallic belt, foremost amongst them being El-Shazly and Afia (1958). They supposed the mineralization to be epigenetic hydrothermal; the hydrothermal having derived from nearby granites. On the other hand, Gad (1978) assigned a volcanogenic origin to these deposits.

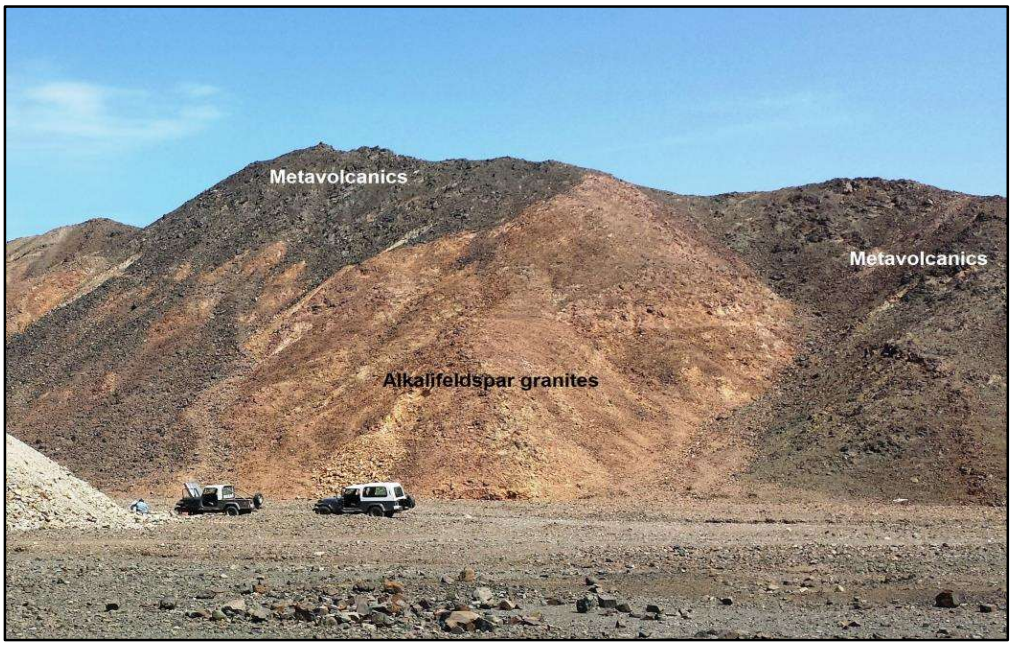


Fig.5 Alkali feldspar granites intrude the island arc metavolcanics.

## METHODOLOGY

To estimate this study we integrating geology, remote sensing, and ground geophysical measurements were used to prospecting, for mineralization, especially gold and associated minerals. However, the presence of gold in pyritic alteration zones could not be directly detected due to unusual geophysical signatures.

**1- Remote Sensing Data**

***The Principal Component Analysis (PCA)***

The PCA is a dynamic method in the mapping and distinguished of rock units (Sobky et al. 2020 and Zaghlol et al. 2021).

The PCA data was computed for the Landsat 8 by using ENVI 5.3 software program to yield the best PCA for the differentiation between rock units.

The best selected PCA composites were PCA 412 in RGB. The PCA (412) is good in differentiating between the different rock assemblages of the current area, especially Metavolcanics (pale green color), Dokhan volcanics (Green color), Hammamat sediments (White color) and older granites (arc granites) which appear in mainly orange as well as monzo to alkali-feldspar granites are red color while younger gabbros are peridot green (Fig.6).

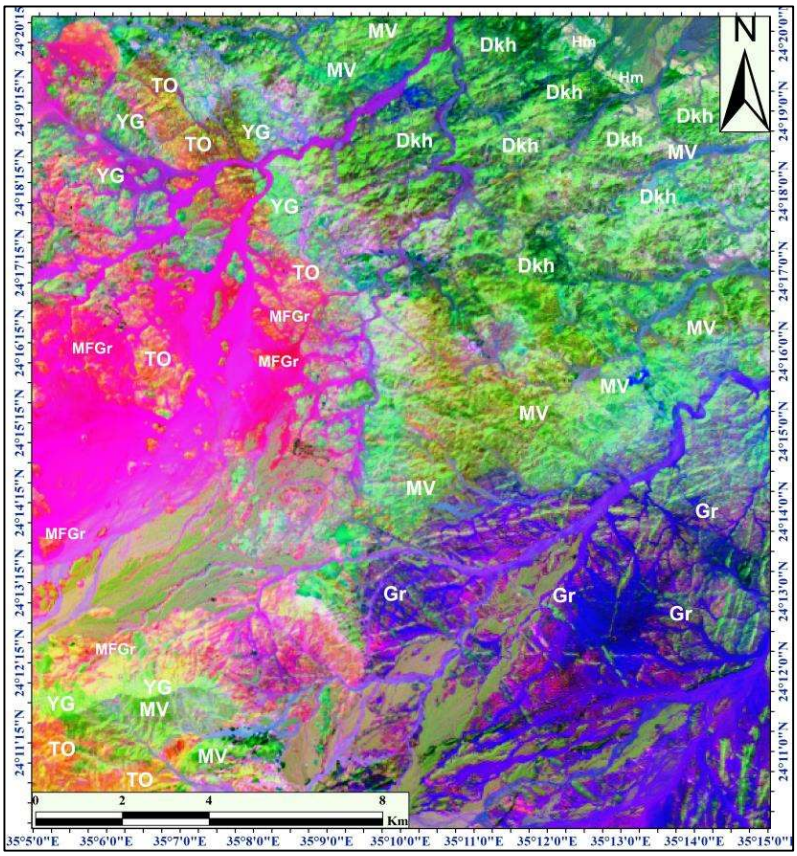


Fig.6 Principal component analysis (PCA) (PC4, PC1, PC2 in RGB) processing and interpretation of Landsat 8 OLI,

Note: MV= metavolcanics, TO = Tonalite, Gr = granodiorite, Dkh = Dokhan volcanics, Hm = Hammamat sediments, YG = Younger gabbros, and MFGr = Monzo and Alkali feldspar granites.

***Color Ratio Composites (Band Ratio)***

Band ratios (BR) are used to remove the topographic variation, and the brightness difference associated to variation of grain size (Sultan et al., 1987). BRs have been used widely in lithological mapping discrimination. Band selection for the different ratio images is used depending on the distinguished spectral signature for rock forming minerals. When rationing methods are applied to Landsat images, all the grouping of minerals are best discriminated by a combination of ratios that include short wavelength bands (i.e. 3/1, 4/1 and 4/2). The ratio of the bands has long-wavelength (5/7) and a ratio of the long to short-wavelength band, (e.g. 5/4 or 5/3) (Crippen, 1989).

The band ratios 7/6, 7/5 and 5/3 (Fig.7) used to discriminating granitic intrusions (mainly pink and light blue colors), metavolcanics (yellow to yellowish green colors) and Dokhan volcanics (mainly light purple color). Band ratio 4/5, 5/7 and 3/1 (Fig.8) proved to be more effective in detection metavolcanics in purple to red color, Dokhan volcanics in green color where the gabbroic rocks in orange color. In addition, some authors used the band ratio images as a useful, powerful technique for lithologic detailed mapping. In 1987, Sultan et al., used the band ratios (b6/ b7) for hydroxyl content

index, and (b6/b2) for opaque phases and high Ferric-aluminous silicates rocks of Landsat 8 OLI data. Moreover, Hassan et al. (2017) used ratios (b6/b4) to discriminate the hydroxyl-bearing rocks and the band ratio (b4/b2) to successfully differentiate mafic rocks such as gabbros (Fig.9).

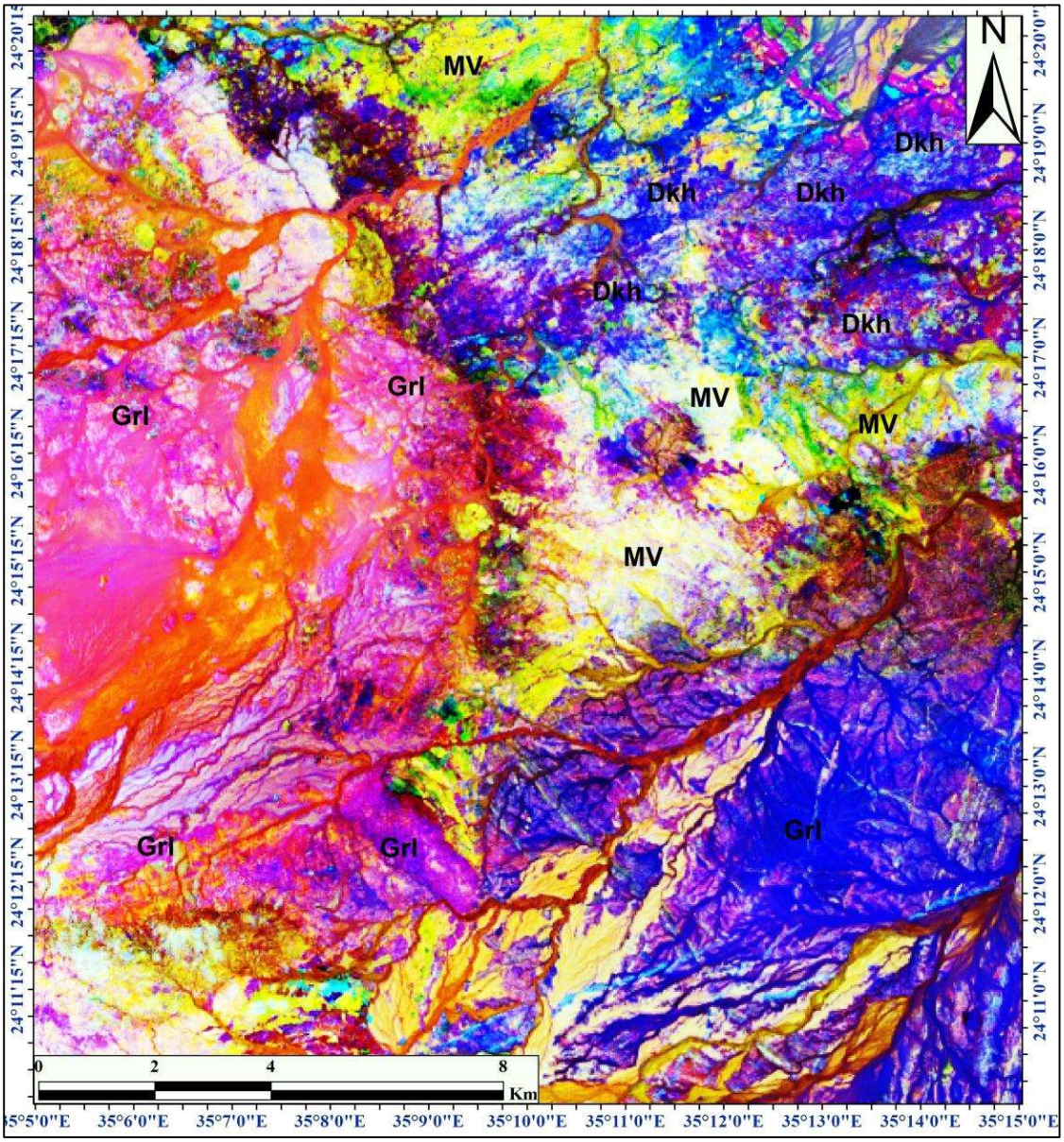


Fig.7 Band ratios (BR) (7/6, 7/5, 5/3 in RGB) Image processing and interpretation

Note: MV= metavolcanics, Dkh = Dokhan volcanics, GrI = Granitic intrusions

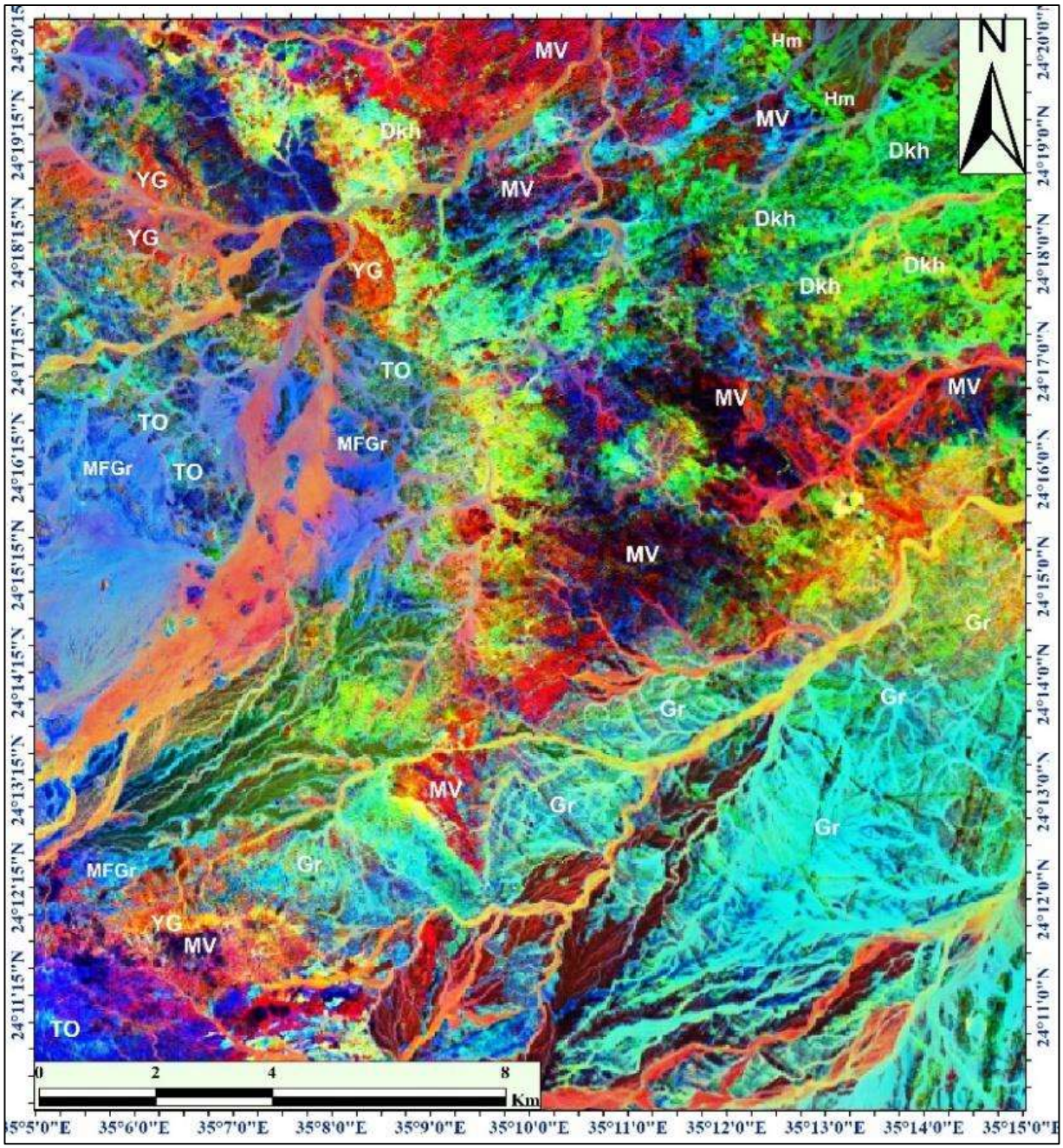


Fig.8 Band ratios (BR) (4/5, 5/7, 3/1 in R, G and B) Image processing and interpretation

Note: MV= metavolcanics, TO = Tonalite, Gr = granodiorite, Dkh = Dokhan volcanics, Hm = Hammamat sediments, YG = Younger gabbros, and MFGr = Monzo and Alkali feldspar granites.

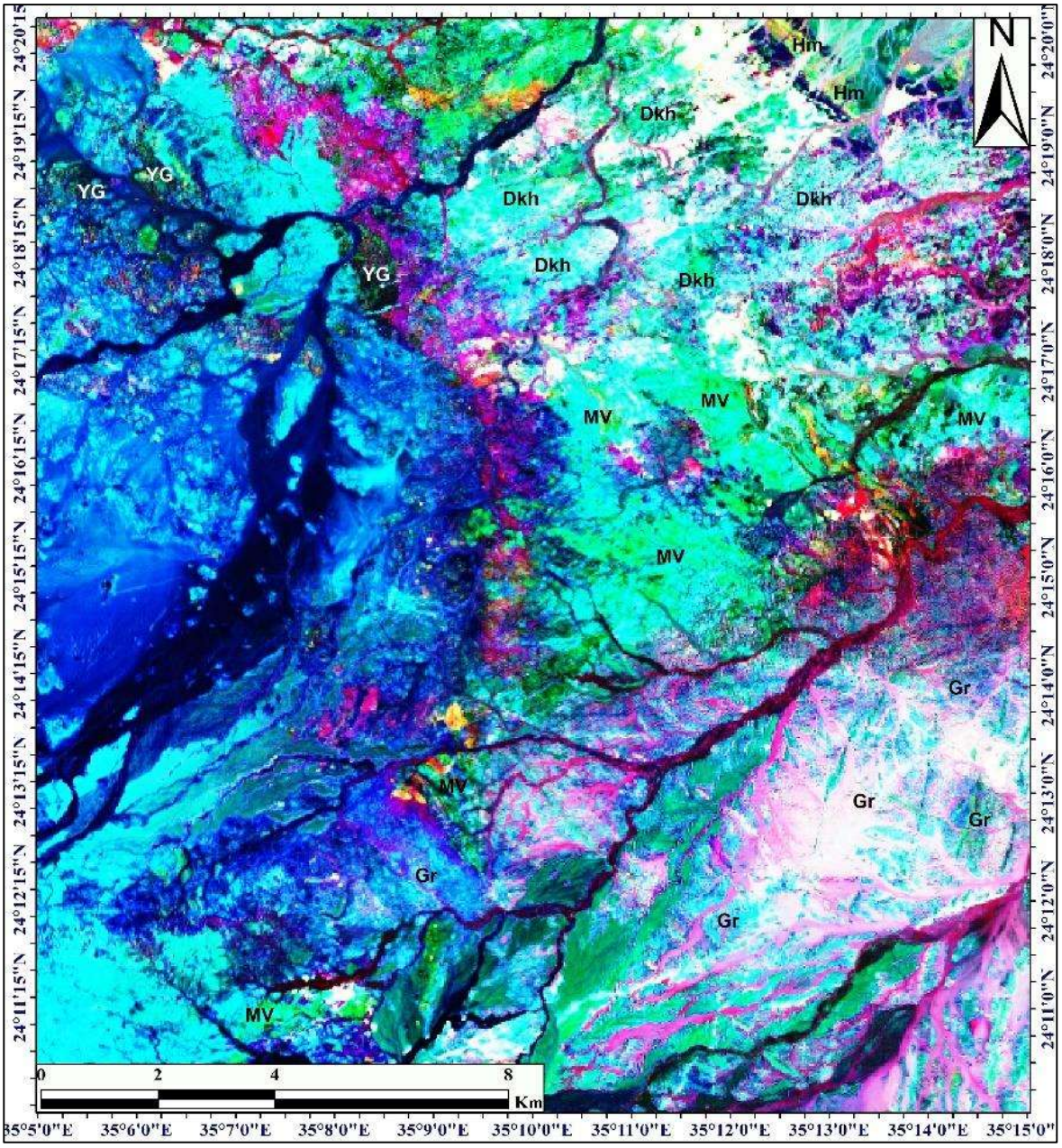


Fig.9 Band ratios (BR) (6/7, 6/2, 4/2 in RGB) Image processing and interpretation

Note: MV= metavolcanics, Dkh = Dokhan volcanics, Hm = Hammamat sediments, YG = Younger gabbros, and Gr = granitic rocks

***Image Classification***

Image classification is considered the most significant remote sensing techniques, for mapping and mineral exploration. Classification is the procedure by which pixels have similar spectral features and consequently, assumed to belong to the similar group that can identified and assigned a same color.

There are two ways to perform the classification: supervised and unsupervised classifications (Muthukrishnan, 2002).

***1- Unsupervised Classification***

This technique sets the pixels into groups depend on the distribution in the image. Unsupervised classification technique may require the specify a number of classes, a maximum number of iterations and a threshold rate.

ENVI 5.3 software package was used in K-Means unsupervised classification. K-Means classification computes initial class means evenly distributed throughout the data space then iteratively groups the pixels into the nearest class using a minimum distance method.

In the current study, the unsupervised k-means classification is conducted in the Landsat-8 images (OLI) data, where the number of classes is (10), the maximum number of iteration (40) and the threshold value is 95% to produce the unsupervised classification for area under the study (Fig.10). Result was found mainly good, so the unsupervised classification is usually useful for mapping the different rocks in the current study.

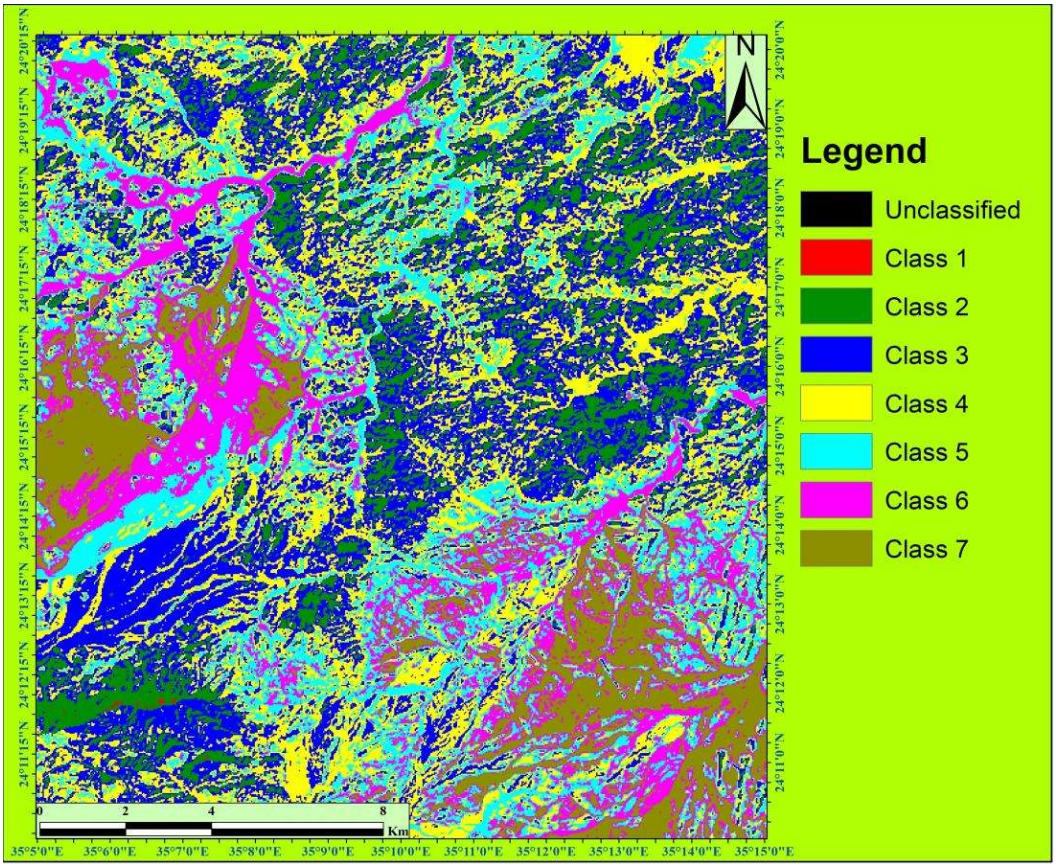


Fig.10 The unsupervised classification Image processing and interpretation.

### *2- Supervised Classification*

This technique contains a significant number of inputs from the image analyst and information about the natures of surfaces that are found within the investigated area. This data can be gathered from previously published maps, or from field work where different surface types are recognized then input into the software as Regions of Interest (ROIs). The computer generates statistical parameters from the (ROIs) and compares the digital numbers of every pixel in the image with these statistical parameters. If the digital numbers for a pixel fall within a known training area, then the pixel is supposed to belong to the same surface class as the training area. After the classification process has taken place different colors representing different surface classes will be assigned.

In existing research, the supervised classification is done (Fig.11), whereas the collecting samples are made using Region of Interest (ROI). ROI is used for more precision in collecting samples; We collect more than 12 rock samples from different localities in the present study with about 110 training samples collected from rock units cropping out. These samples are evaluated using histogram, signature mean plot and signature alarm methods for detecting the overlap zones between the collected samples

in different bands, the supervised classification has been used to classify the image for land cover classification.

The equation computes the statistical probability of a pixel fitting to an exact signature. Also, Maximum likelihood classifiers will label all pixels in an image. The Maximum Likelihood parametric rule was used in the present study because it is more precise mean to get supervised classification for different rock units' types (Fig.11); eight classes are allocated to eight colors each is corresponding to a sure rock unit.

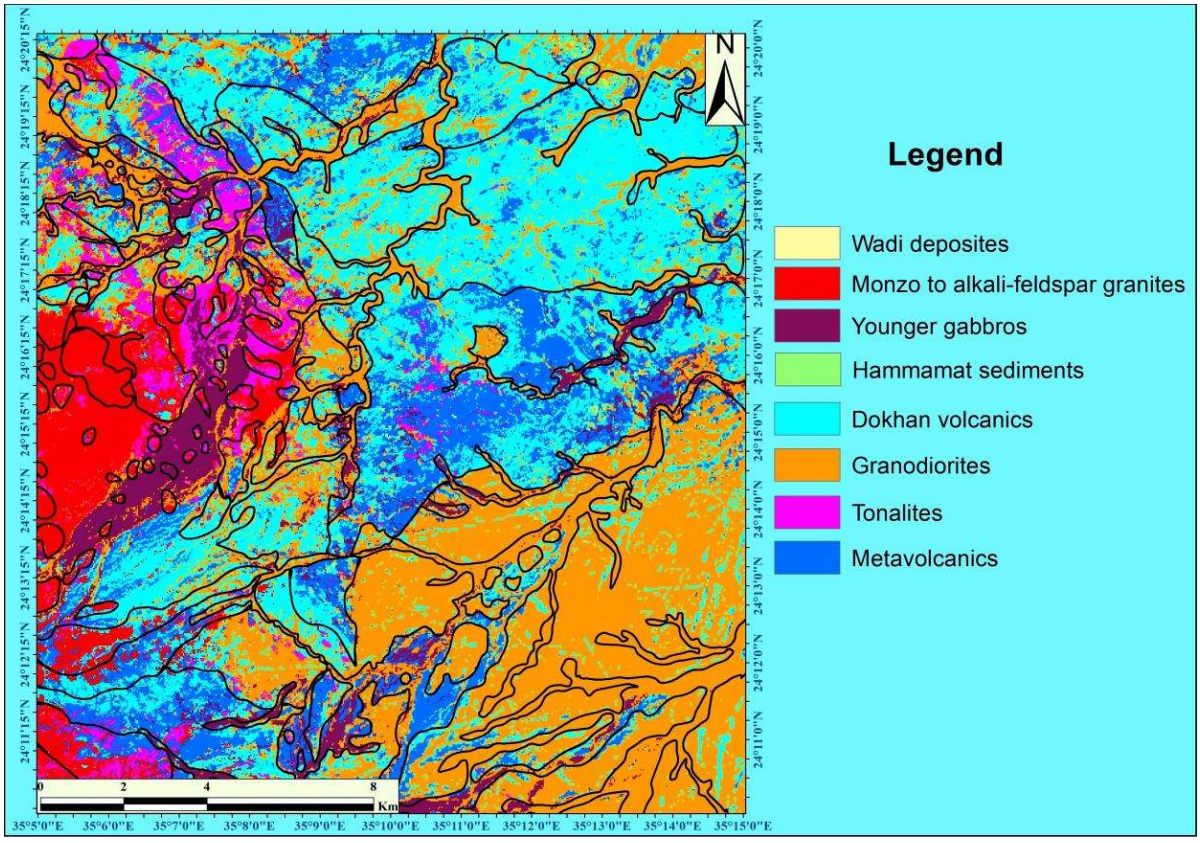


Fig.11 The supervised classification Image processing and interpretation.

**2-Geophysical Studies**

Eleven profiles were acquired in the study area. The profile extensions were 500 meters in length and trend in the NNW direction, in addition to, 2-D detailed geoelectrical profiles were performed at the anomaly zones.

***Reduced to the northern pole (RTP) of magnetic measurements***

Figure (13) shows that different locations of magnetic anomalies of RTP map with different magnitudes and distinct characteristics. Low magnetic anomalies (around 40700 nT) are found in the northwestern and south sections. In contrast, high magnetic potentialities (up to 41563 nT) are concentrated in the central, southeastern and southwestern parts, these high magnetic anomalies correspond to metavolcanic rocks( highly altered rocks) (see Fig.2), which contains sulfide mineralization and gold-related minerals. These low-anomaly zones are bordered by higher magnetic values, interpreted as contact zones and major lineaments trending NE-SW and N-S.

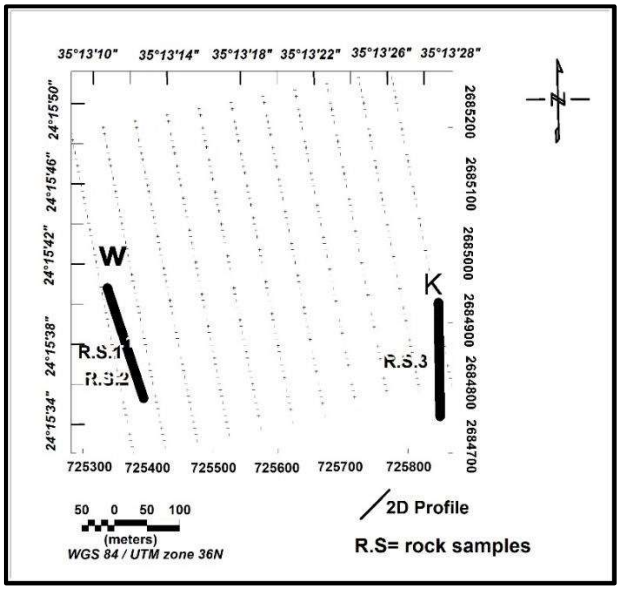


Fig.12 Geophysical measurement stations with 2-D profiles

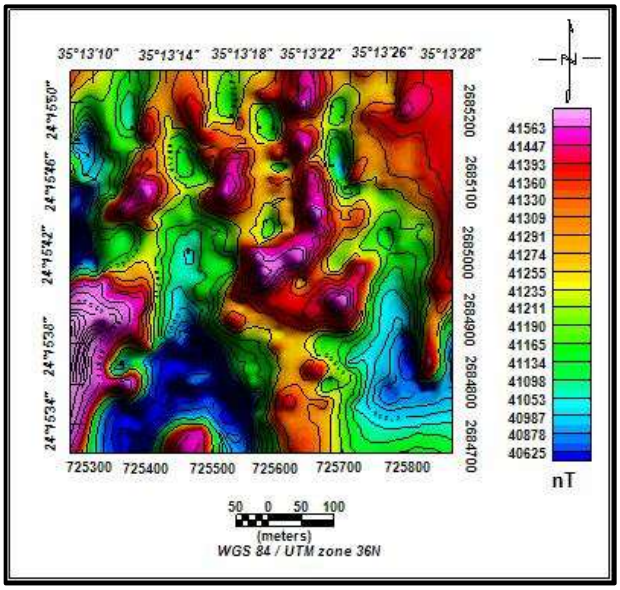


Fig.13 RTP magnetic map.

***The low-pass (regional) and high-pass (residual) magnetic maps***

The residual map (Fig.14) displays alternating positive and negative magnetic zones, also aligned NE-SW and E-W. This map is very important as it gives us a clear picture of the found rock units, which have high magnetic potentialities related to highly fractured metavolcanic rock as they contain sulfide mineralization. With removal of shallow anomalies gives us deep or regional map (Fig.15) with interface level about (30-35m). This map shows that low anomaly locates in the central western and south parts, while high anomaly found in the southwestern and middle parts with structural lineaments, NE-SW and NW-SE trends.

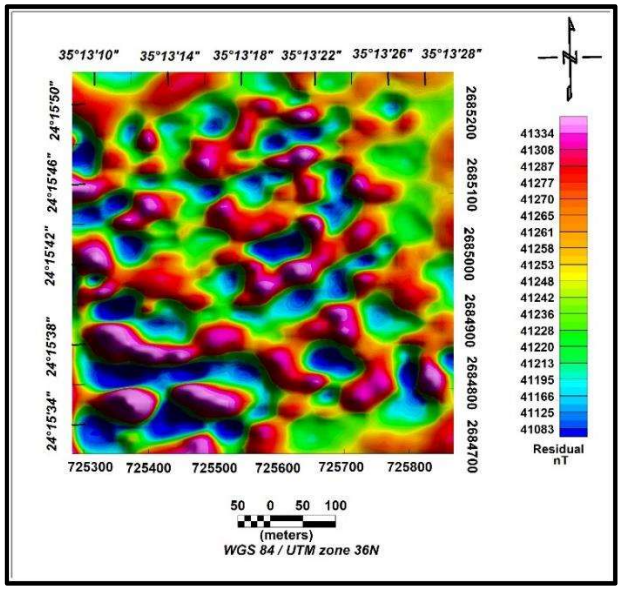


Fig.14 High-pass magnetic map

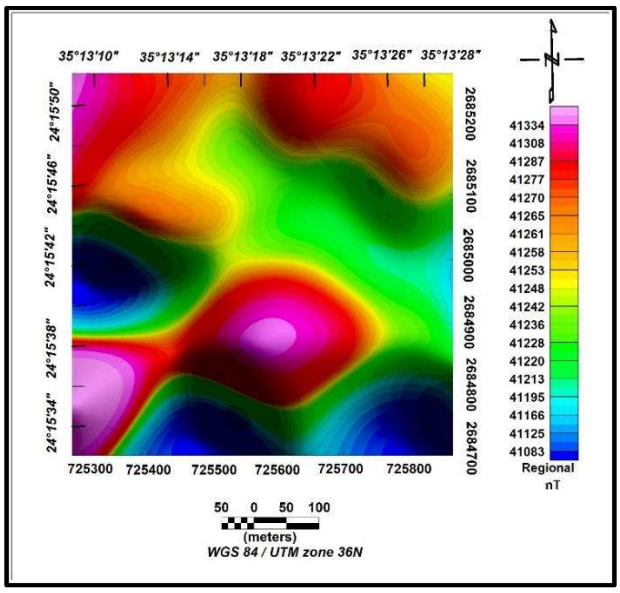


Fig.15 Regional magnetic map

***Self-Potential (SP)***

The SP map (Fig.16), shows negative anomalies lies in the southeastern, western and southern parts which compatibility with high magnetic anomaly zones (see Fig.13), and these anomalies are related to metavolcanic rocks, which containing high percentage of sulfide minerals.

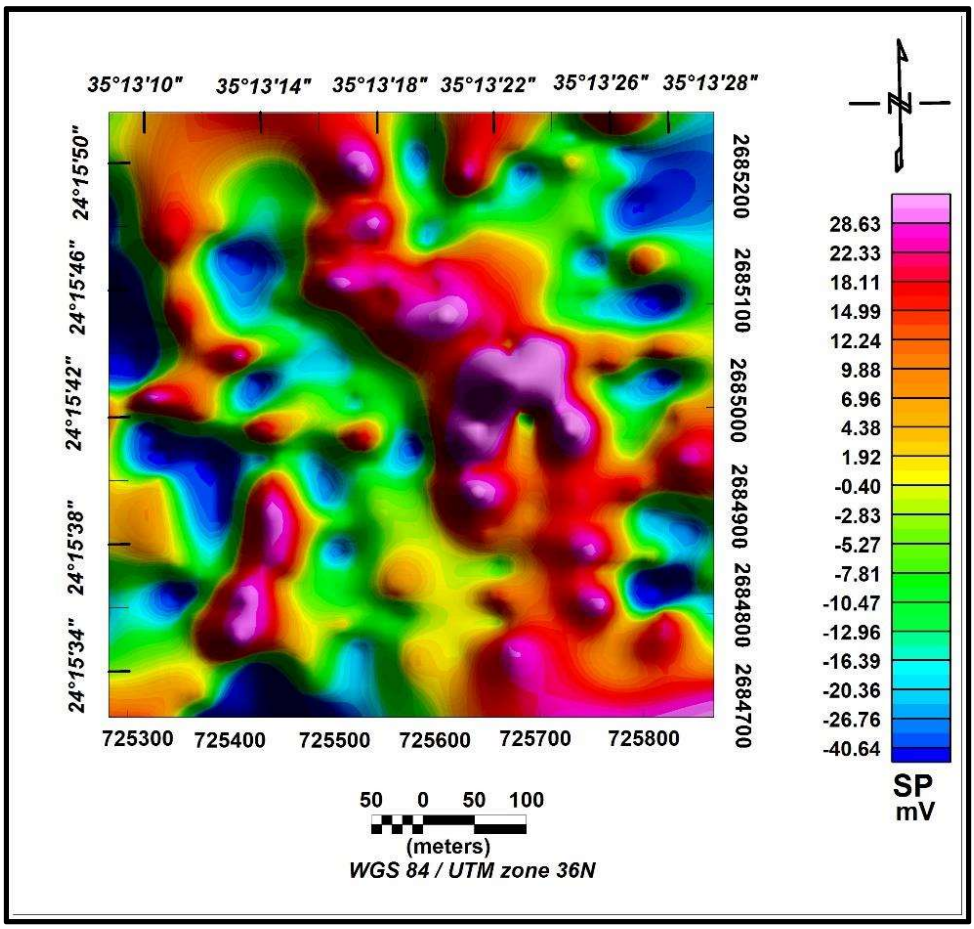


Fig.16 Normal self-potential (SP) anomaly map

***Resistivity/IP -Wenner- Schlumberger profiles (W, K)***

Is a combined between the Wenner and Schlumberger arrays (Pazdirek and Blaha, 1996) rising out of relatively recent work with electrical surveys.

Two- dimensional electrical imaging tomography surveys are applied using many electrodes, 25 or more, connected to a multi-core cable (Griffiths and Barker 1993).

In this research, the location of 2-D Wenner-Schlumberger array profiles (Fig.17) with 32 electrodes connected to two multi-core cables 80 m long was applied to recording measurements.

The inversion was then carried out to detect the true resistivity. The inversion technique of the least square was used to allow the modeling of relatively sharp changes in resistivity/IP because the inversion algorithm aims to minimize the absolute value of data misfit (Loke and Dahlin, 2002).

***1- Geo-Electric Section along Profile (W)***

The profile length is about 155 m and its depth is about 31m (Fig.18), which is located at the southwestern part, and shows that three zones of high chargeability and low resistivity. The first one is found that at a distance of about 90 m from starting of the profile within a depth range of 20–25 m, while the second causative body appears at distance of about 100 m at a depth about 5–6 m and the third ore body appears at a distance of about 120 m of the section with depth about 10- 15m.

***2- Geo-Electric Section along Profile (K)***

The profile length is about 155 m and its depth is about 30m (Fig.19), which is lies at the southeastern part, and shows that three places of low resistivity and relatively high chargeability. The first one there is at a distance of about 85 m with a depth from 24 to 28 m, while the second ore body appears at a distance of about 93 m within a depth range of 8–10 m and the third zone of high

chargeability-low resistivity detected at a distance of about 135 m of the section within a depth about 6- 8 m

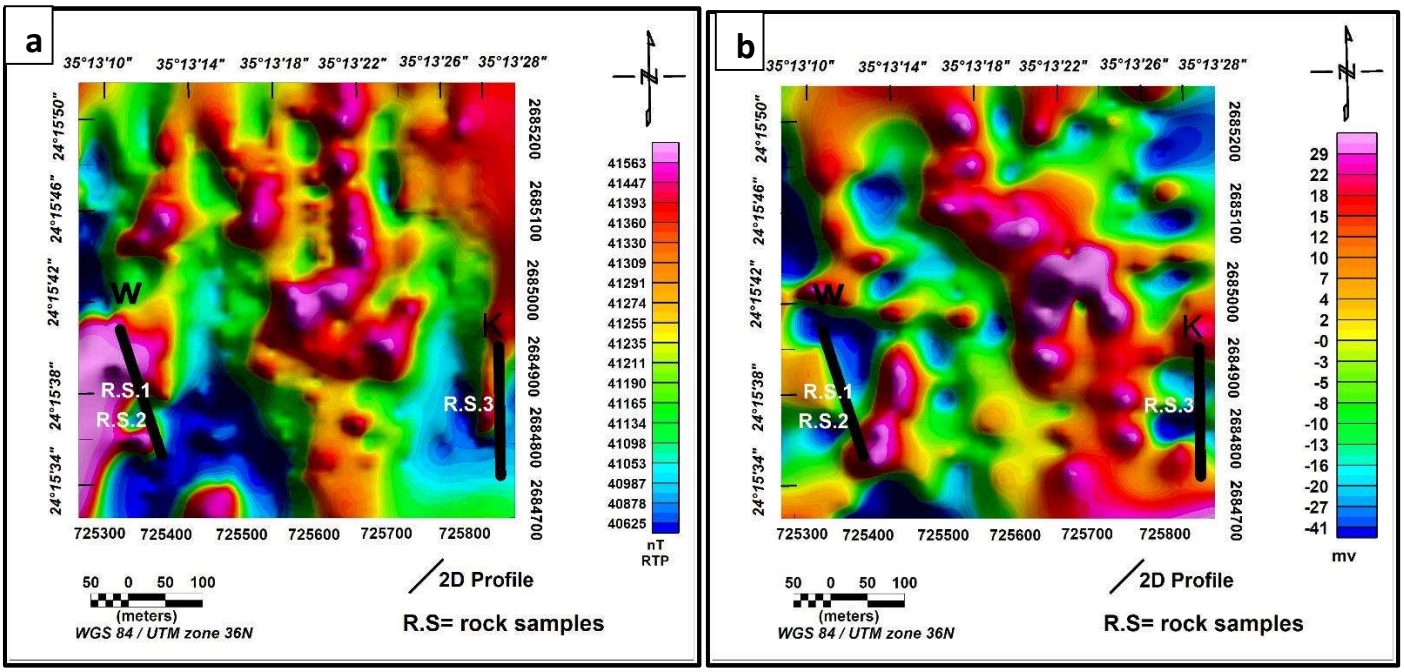


Fig.17 location map of 2-D Wenner- Schlumberger profiles: (a) RTP, (b) SP maps.

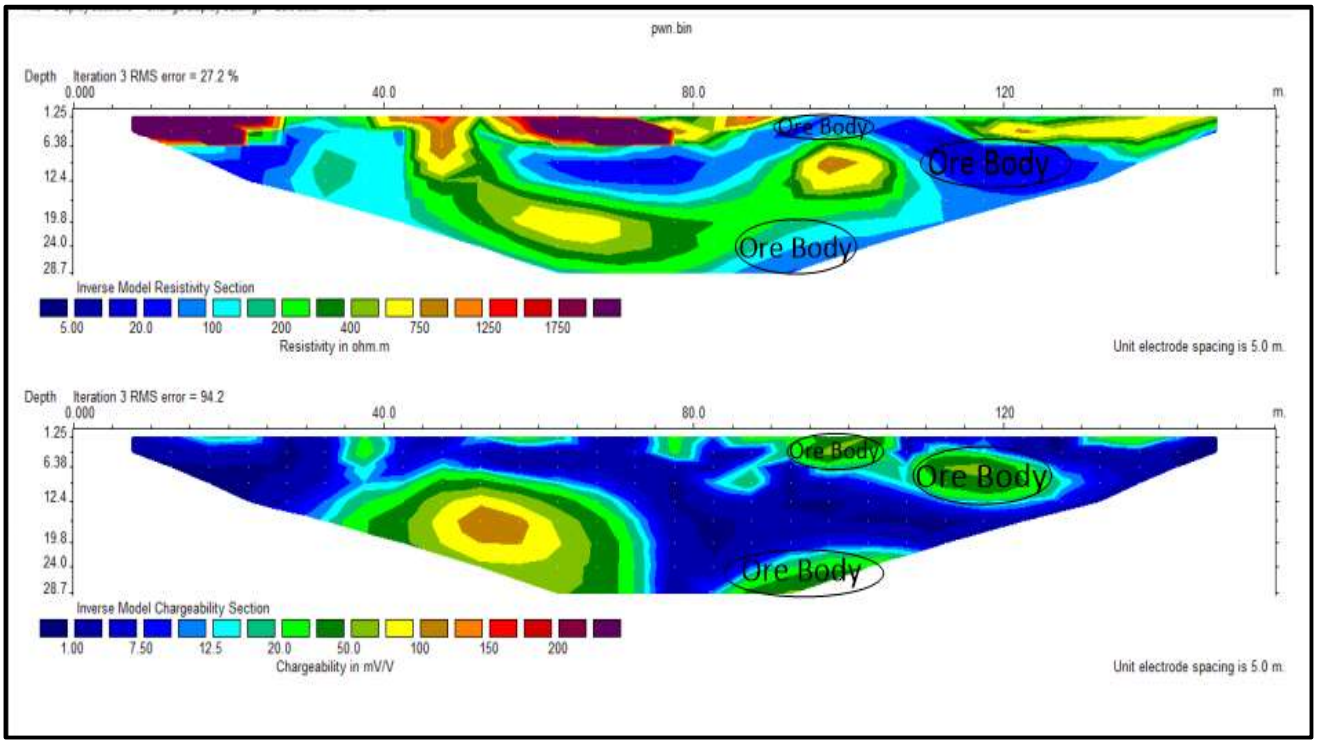


Fig.18: Wenner- Schlumberger array along profile (W)

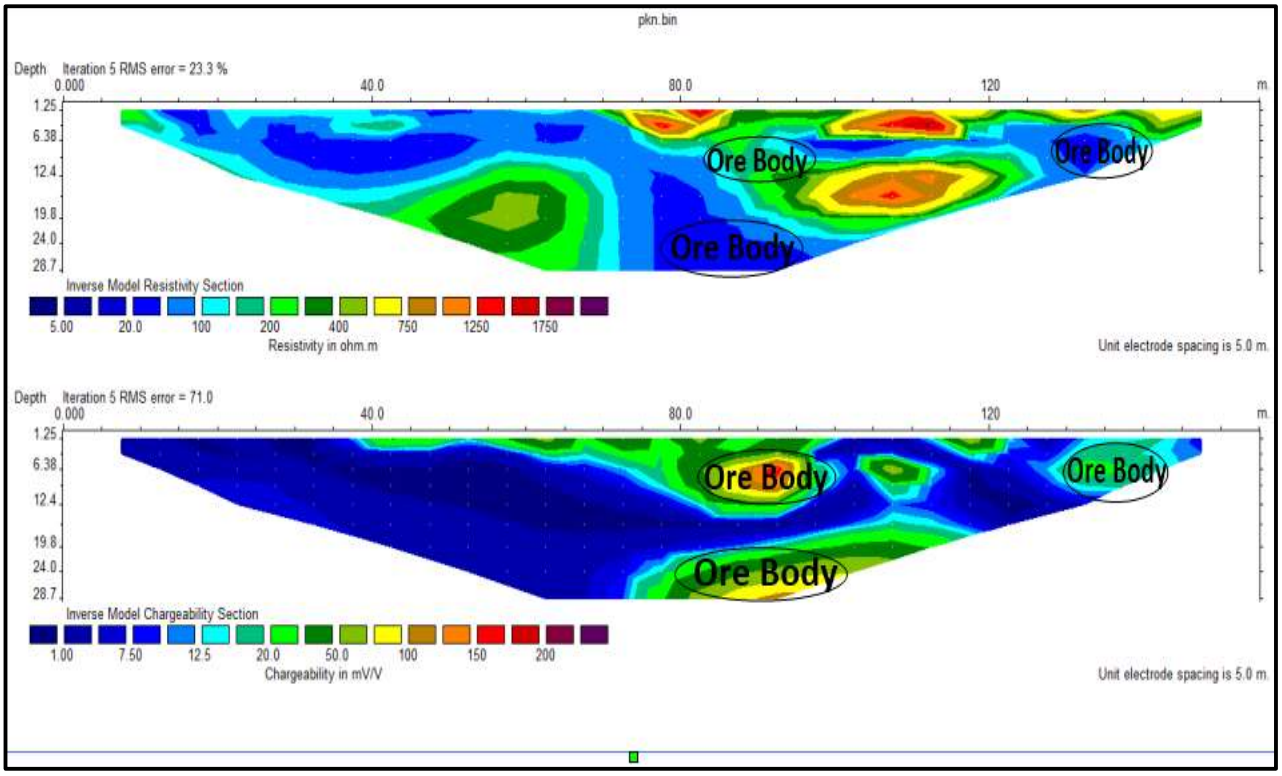


Fig.19 Wenner- Schlumberger array along profile (K)

## Integration of results

1) Correlation between RTP and SP maps

Figure (17) shows the connection between RTP and SP maps, this figure indicates that; high magnetic and low SP anomalies, which could reflect the mineralized zones.

2) Analyses of several samples

Table (1) gives a brief summary of several samples that associated with Au, Ag, Cu, Pb and Zn mineralization and related to anomaly zones and located at 2D Geo-electric cross sections.

Table 1. Location of samples and analyses of them in prospecting area with ppm unit.

| R.S | X | Y | Au ppm | Ag ppm | Cu ppm | Pb ppm | Zn ppm | Notes |
|---|---|---|---|---|---|---|---|---|
| R.S.1 | 725387.8 | 2684860 | 0.6 | 1.5 | 6.1 | - | - | Profile W |
| R.S.2 | 725387.8 | 2684900 | 0.3 | 0.6 | 44.3 | - | - | Profile W |
| R.S.3 | 725850 | 2684840 | 0.6 | 1.1 | 17.3 | 18 | 119.5 | Profile K |

## RECOMMENDATION

The obtained results from this study may lead to the following recommendations:
detailed geological survey, drilling wells and geochemical analyses at the western, southeastern and central parts of the study area.

## CONCLUSIONS

The combined analysis of geological, remote sensing results and geophysical data in this research delivers significant information about the determination of mineral resources especially gold mineralization and associated minerals which, related to disseminated sulfides in metavolcanic rocks, that may be structurally controlled.

## REFERENCES

**Abu El-Leil, I., (1990):** Petrogenesis and tectonic evolution of some metagabbro-gabbro association, central Eastern Desert, Egypt. Al-Azhar Bulletin of Science Vol.1 No.1-2, pp. 57-68, 1990.

**Abu El-Rus, M.A. (1991):** Geological Studies on Abu Ghalaga Area, Eastern Desert, Egypt, M.Sc. Thesis, Assiut University, 255p.

**Akaad, M.K. and Noweir, A.M., 1980,** Geology and Lithostratigraphy of the Arabian Desert Orogenic Belt of Egypt Between Latitudes 25º 35` and 26º 30` N, I.A.G. Bull., Jeddah, 2, 127- 136.

**Crippen, R. E., (1989):** Development of remote sensing techniques for the investigation of nontectonic activity, eastern Transverse Ranges and vicinity, southern California, Ph. D. thesis, University of Calif., Santa Barbara, 304P.

**Egyptian Geological Survey and Mining Authority (EGSMA, 1997):** Geologic Map of Jabal Hamata Quadrangle, Egypt, Scale 1:250000.

**El Ramly, M.F. and Akaad, M.K. (1960):** The Basement Complex in the Central Eastern Desert of Egypt between Latitudes 24º 30` and 25º 40` N. Geol. Surv. Egypt, Paper No.8, 35p.

**El Sobky MA, Madani AA, and Surour AA., (2020),** Spectral characterization of the Batuga granite pluton, south Eastern Desert, Egypt: influence of lithological and mineralogical variation on ASD Terraspec data. Arab J. Geosci. 13 (23), 1-15p.

**El-Bialy, M.Z., (2010):** On the Pan-African transition of the Arabian–Nubian Shield from compression to extension: The post-collision Dokhan volcanic suite of Kid-Malhak region, Sinai, Egypt. Gondwana Research 17, 26-43.

**El-Gaby, S., List, F. K. and Tehrani, R., (1988):** Geologic evolution and metallogensis of the Pan-African belt in Egypt. In: El-Gaby, S. and Greiling, R. O. (eds): The Pan-African belt of Northeast Africa and adjacent areas. Vieweg and Sohn, Braunschweig / Wieshbaden. pp. 17-68.

**Elnazer, A. A., Azer, M. K., Mohamed, Y. M. A. & El Nazer, H. A., 2022,** Comparative efect of the three talc deposits in detoxifcation of Cr (VI) from wastewater. Int. J. Environ. Sci. Technol. https://doi.org/10.1007/s13762-022-04475-3.

**El-Ramly, M.F. (1972):** A New Geological Map for the Basement Rocks in the Eastern and Southwestern Deserts of Egypt, Annals of the Geological Survey of Egypt 2, 1-18.

**El-Shazly, E. M., and Afia, M. S. (1958):** Geology of Samiuki deposit, Eastern Desert: Egypt. J. Geol. v.2 N. 1, p.27-45.

**El-Shazly, E.M., 1964.** On the classification of the Precambrian and other rocks of magmatic affiliation in Egypt. Proceeding of the 22th International Geology Congress, New Delhi, 10, 88-101.

**Gad, M.A., Soliman, F., Halim, E.A., Fakahry, R., Gad, V.D., and Soliman, Kh.A, (1978):** Geology and geochemical exploration of Hamata area. Internal reports No. 86/78, Geol. Surv. Egypt. 44p.

**Griffith D.H. and Barker R.D. (1993):** Two-Dimensional Resistivity Imaging and Modeling in Areas of Complex Geology, Journal of Applied Geophysics, 29, 211-226.

**Hamdy, M. M., Lasheen, E. S. R. & Abdelwahab, W., 2022,** Gold-bearing listwaenites in ophiolitic ultramafcs from the Eastern Desert of Egypt: Subduction zone-related alteration of Neoproterozoic mantle? J. Afr. Earth Sci. 193, 104574.

**Hassan, A. M. and Hashad, A. H., (1990):** Precambrian of Egypt. In: The Geology of Egypt (Edited by Said, R.) Balkema, Rotterdam, Brookfield. pp. 201-248.

**Hassan, S.M., Sadek, M.F., 2017.** Geological mapping and spectral based classification of basement rocks using remote sensing data analysis: The Korbiai-Gerf nappe complex, South Eastern Desert, Egypt. Journal African Earth Science, 134, 404–418.

**Loke, M.H., and Dahlin, T. (2002):** A Comparison of the Gauss Newton and Quasi-Newton Methods in Resistivity Imaging Inversion of Applied Geophysics, 49, 149-162

**Masoud, M.S., 1994,** Geological map of sheikh shadli-Hamata district, south eastern desert, Egypt. Internal report 36/94, Geol. Surv. Egypt, Cairo.

**Mostafa, M.o.,1996,** Geological map of Tarafawi-Abu Ghusun area, south eastern desert, Egypt. Internal report 2/96, Geol. Surv. Egypt, Cairo.

**Muthukrishnan, S., (2002): "Lab-5**: Environmental Impact Analysis Project II: Classification unSupervised" http://www.eas.purdue.edu/eas591f/Detailed_ schedule.html

**Pazdirek, O. and Blaha, V. (1996):** Examples of Resistivity Imaging Using ME100 Resistivity Field Acquisition System. EAGE 58th Conference and Technical Exhibition Extended Abstracts, Amsterdam.

**Shukri, N.M., and Mansour, M.S. (1980):** Lithostratigraphy of Um Samiuki District, Eastern Desert, Egypt, Inst. Appl. Geol. Jeddah Bull., No.4, V. 3,127- 134.

**Sultan, M., Arvidson, R. E., Sturchio, N. C. and Guinnes, E. A., (1987):** Lithologic mapping in arid regions with Landsat TM data: Meatiq dome, Egypt. Geological Society of America Bulletin, Vol. 99, pp. 748-762.

**Zaghlol Kh, Sakran Sh, El-Sharkawi MA, and Said A., (2021),** Petrographical, structural, and remote sensing–based mapping of Gebel Atawi area, central Eastern Desert, Egypt. Arab J. Geosci. 14 (1368).